Science and Technology of Advanced Materials

ISSN: (Print) (Online) Journal homepage: www.tandfonline.com/journals/tsta20

Ball-milled MoS_2 with graphene shows enhanced catalytic activity for hydrogen evolution reaction

Linghui Li, Satish Laxman Shinde, Takeshi Fujita & Takahiro Kondo

To cite this article: Linghui Li, Satish Laxman Shinde, Takeshi Fujita & Takahiro Kondo (29 May 2024): Ball-milled MoS_2 with graphene shows enhanced catalytic activity for hydrogen evolution reaction, Science and Technology of Advanced Materials, DOI: 10.1080/14686996.2024.2359360

To link to this article: https://doi.org/10.1080/14686996.2024.2359360

© 2024 The Author(s). Published by National Institute for Materials Science in partnership with Taylor & Francis Group.

View supplementary material

Accepted author version posted online: 29 May 2024.

Submit your article to this journal

View related articles

View Crossmark data

Full Terms & Conditions of access and use can be found at https://www.tandfonline.com/action/journalInformation?journalCode=tsta20

Check for updates

Publisher: Taylor & Francis & The Author(s). Published by National Institute for Materials Science in partnership with Taylor & Francis Group.

Journal: *Science and Technology of Advanced Materials*

DOI: 10.1080/14686996.2024.2359360

ACCEPTED MANUSCRIPT

Ball-milled MoS_2 with graphene shows enhanced catalytic activity for hydrogen evolution reaction

Linghui Li [a], Satish Laxman Shinde [b,c], Takeshi Fujita [d], and Takahiro Kondo [b,e,f*]

[a] *Graduate School of Pure and Applied Sciences, University of Tsukuba, Tsukuba 305-8573, Japan*

[b] *Department of Materials Science, Institute of Pure and Applied Sciences, University of Tsukuba, Tsukuba 305-8573, Japan*

[c] *Department of Physics, Indian Institute of Technology Hyderabad, Kandi, Telangana, 502284, India*

[d] *School of Engineering Science, Kochi University of Technology, Kochi 782-8502, Japan*

[e] *Tsukuba Research Center for Energy Materials Science, Institute of Pure and Applied Sciences and R&D Center for Zero CO_2 Emission with Functional Materials, University of Tsukuba, Tsukuba 305-8573, Japan*

[f] *Advanced Institute for Materials Research, Tohoku University, Sendai 980-8577, Japan*

[*] Corresponding author. E-mail address: takahiro@ims.tsukuba.ac.jp (T. Kondo).

ABSTRACT

The hydrogen evolution reaction (HER) is an important phenomenon in water splitting. Consequently, the development of an active, earth-abundant, and inexpensive HER catalyst is highly desired. MoS_2 has drawn considerable interest as an HER catalyst because it is composed of non-precious metal and exhibits high catalytic activity in the nanosheet form. In this study, size-controlled MoS_2 particles were synthesized by ball milling. The as-prepared samples exhibited significantly enhanced electrochemical and catalytic properties compared to those of pristine bulk MoS_2. Furthermore, the HER activity improved further upon the introduction of graphene into the as-prepared ball-milled samples. In particular, the MoS_2 sample ball-milled for 12 h mixed with graphene exhibited optimal performance, showing an overpotential (160 mV at 10 mA cm^{-2}) that was ~335 mV lower than that of pristine bulk MoS_2. The superior catalytic activity was ascribed to the exposed edge sites, sulfur vacancies, and 1T phase of MoS_2, as well as the noteworthy fortifying effect of the electronically conductive flexible material, graphene. The results provide a promising strategy for its application as an efficient and stable HER catalyst.

KEYWORDS: molybdenum disulfide; hydrogen evolution reaction; electrocatalyst; edge site; 1T phase; sulfur vacancy

1. Introduction

The adverse impact of fossil fuels on the environment and the need to sustainably advance human society have led to a recent focus on replacing fossil fuels with renewable energy [1]. To that end, hydrogen has been promoted as an ideal energy carrier since the early 1970s because of its high weight energy density and zero CO_2 emissions [2]. Hydrogen can store the energy generated by renewable sources in chemical bonds and convert it back into electricity when needed through fuel cells or other devices. Hydrogen is mainly present in compounds such as

ACCEPTED MANUSCRIPT

hydrocarbons and water on our planet and is primarily obtained through energy-intensive greenhouse-gas-emitting processes, such as the steam reforming of hydrocarbons [3]. However, achieving sustainable and economically feasible hydrogen production on an industrial scale is a major challenge [4]. One way to address this issue is to decompose water through electrolysis or photocatalysis, using renewable solar energy to separate water molecules directly or indirectly into their components [5,6].

The hydrogen evolution reaction (HER) is an extensively studied electrochemical process that involves the cathodic half-reaction of water decomposition [7]. It plays a crucial role in various energy-conversion devices, including hydroelectric and artificial photosynthetic cells. As its name suggests, the HER involves the reduction of protons or water molecules, leading to the release of gaseous hydrogen, as follows [8]:

$$2H^{+}_{(aq)} + 2e^{-} \rightarrow H_{2(g)}, \qquad (1.1)$$

where (aq) and (g) denote the form of H_3O^+ species in the aqueous solution and the gas phase, respectively. The standard reduction potential of the HER is defined as $E^{0}_{H^+/H_2} = 0\,V$ *versus* a normal hydrogen electrode (NHE) at pH 0. However, similar to many chemical reactions, the electrochemical processes occurring during the HER must overcome a certain activation energy barrier (that is, the overpotential) to proceed. Electrocatalysts are typically required to reduce the overpotential, thereby improving the reaction rate and efficiency.

High-performance catalysts for the critical electrochemical HER should minimize the overpotential and thereby enhance its efficiency. Pt-group metals are considered remarkably

ACCEPTED MANUSCRIPT

efficient HER electrocatalysts. However, the development of HER catalysts with exceptional activity using materials that are more readily available and cost-effective is challenging [9].

Molybdenum disulfide (MoS_2), which has been widely studied as a hydrodesulfurization catalyst, has recently garnered attention as an HER electrocatalyst because of its high catalytic activity [10,11,12]. Both computational and experimental findings have confirmed that the HER activity originates from the edges of the MoS_2 plates [13,14], whereas their basal planes are catalytically inactive. Additionally, recent studies have reported other catalytic active sites of MoS_2 toward the HER. For example, MoS_2 with the 1T structural phase exhibits high catalytic activity, even with substantial oxidation at the edge sites [12,15,16]. Furthermore, the catalytic activity of a MoS_2 film increases with decreasing thickness and is potentially superior to that of edge-rich pyramidal MoS_2 nanosheets [17]. In addition to the edge sites, the sulfur vacancies of MoS_2 provide another set of major catalytically active sites for the HER [15,18]. Consequently, the exposure of more edges, converted to the octahedral (1T) structural phase, and sulfur vacancy engineering are expected to be viable strategies for synthesizing MoS_2 with higher catalytic performance than that of bulk MoS_2 [13,16,19,20].

One limitation of MoS_2 catalysts is that their active sites are limited to edges [21]. To fully harness the potential of MoS_2-based catalysts, there is a pressing need to increase the number of active sites, enhance the activity of these catalytic sites, and improve the electrical connections between the active sites and catalyst substrate [22]. One approach to optimizing charge transfer involves the use of a graphene support, which has been demonstrated to significantly enhance the HER kinetics [12].

ACCEPTED MANUSCRIPT

MoS_2 belongs to the category of quasi-two-dimensional transition metal dichalcogenides with a layered structure, and has recently gained significant attention owing to its unique electronic, optical, optoelectronic, and catalytic properties [23]. In its bulk form, MoS_2 is an indirect-bandgap semiconductor with an energy gap of 1.29 eV, and it comprises multiple layers of S–Mo–S bonds, held together by weak van der Waals interactions. Each layer comprises a central plane of Mo atoms sandwiched between two S atoms, with strong covalent bonds and dipole formation between the positively charged Mo atoms and negatively charged S atoms. The Mo atoms in MoS_2 adopt two different coordination modes: 1T phase and trigonal prismatic (2H and 3R phases), with the 2H phase being the most common in bulk MoS_2. Notably, the crystal system can be exfoliated into individual layers owing to the weak van der Waals forces holding the S–Mo–S layers together [16,24]. These individual layers exhibit properties that differ significantly from those of the bulk material. However, although the conversion of 2H MoS_2 into the 1T phase can lead to enhanced catalytic performance in the HER [25,26], the precise mechanisms underlying this improvement are not fully understood.

Various methods have been developed to chemically exfoliate bulk MoS_2 [16,24,25,27]. One approach involves the use of Li intercalation to construct single- or few-layered structures [23]. Alternatively, a bottom-up approach has been pursued to directly synthesize MoS_2 nanostructures with a high density of edge sites [20,22]. Other methods include the chemical exfoliation of bulk MoS_2 by sonication and solvent utilization [24,28]. Notably, all these methods involve wet-chemical processing schemes and may require potentially hazardous chemicals. Furthermore, chemical exfoliation tends to yield a minuscule amount of exfoliated material. Additionally, scaling up these methods can be challenging in

ACCEPTED MANUSCRIPT

terms of economics, environmental concerns (for example, Li intercalation and solvent use), and technological feasibility (for example, sonication) [19]. In this context, ball milling, a simple and efficient method, shows promise for improving the catalytic properties of bulk MoS_2 [10,19].

In this study, a straightforward and scalable method based on dry ball milling was adopted to synthesize size-controlled MoS_2 with significantly enhanced electrochemical catalytic properties. The original material—pristine bulk MoS_2 powder—was not subjected to any chemical reactions or agents. Comprehensive characterization was performed using techniques such as scanning electron microscopy (SEM), energy-dispersive X-ray (EDX) spectroscopy, and X-ray photoelectron spectroscopy (XPS) to track the morphological and chemical changes that occurred during ball milling. Additionally, the possible introduction of metallic impurities could affect the electrochemical and catalytic properties of the material was probed. Overall, this study was aimed at synthesizing size-controlled MoS_2 with enhanced HER-catalyzing activity by increasing the number of edge sites, introducing the 1T phase, and introducing sulfur vacancies via the simple ball milling method, and examining the effects of each process step on the activity.

2. Materials and Methods

2.1 Materials

MoS_2 bulk powder, graphene nanoplates (GNPs; average number of layers: 5–7), Nafion (5 wt% in lower aliphatic alcohols and water), H_2SO_4 (97%), and commercial Pt/C (20 wt%

ACCEPTED MANUSCRIPT

loading; matrix activated carbon support) were purchased from Sigma-Aldrich (Japan). The solvents were purchased from commercial sources.

2.2 Synthesis of ball-milled MoS_2

A planetary ball mill (Fritsch PL-7, Flitch, Japan) whose container (capacity: 20 cm^3) and balls (diameter: 1 cm) were made of ZrO_2 was used for ball milling. Bulk MoS_2 (100 mg) and six balls were placed in a container, and milling was performed at atmospheric pressure, a temperature of ~300 K, and a rotation speed of 400 rpm. Each cycle involved 5 min of rotation, followed by a rest period of 30 s (to prevent temperature increases during long-term operation). Ball milling was performed for 15 min, 30 min, 45 min, 1 h, 2 h, 4 h, 8 h, and 12 h. The ball-milled samples are denoted herein based on the ball-milling duration; for example, the MoS_2 sample ball-milled for 30 min is named "MoS_2-30 min."

2.3 Preparation of "MoS_2-ball milled + sonicated" ink

Ball-milled MoS_2 powder (5 mg) was suspended in a mixture of ethanol (1 mL) and Nafion (50 µL), and the resulting sample was subjected to 2 h of bath sonication (500 W / 60 Hz, AS ONE Ltd., Japan), yielding a sample denoted as "MoS_2-ball milled + sonicated" herein.

2.4 Preparation of "MoS_2-ball milled + G" ink

Ball-milled MoS_2 powder (5 mg) and GNPs (10 mg) were suspended in ethanol (1 mL) and then underwent 1 h of bath sonication (500 W / 60 Hz, AS ONE Ltd., Japan). A Nafion solution (50 µL) was added to the resulting mixture to prepare the ink for electrochemical measurements, denoted herein as "MoS_2-ball milled + G."

ACCEPTED MANUSCRIPT

2.5 Characterization

Powder X-ray diffractometry (XRD) was performed using a Rigaku MiniFlex instrument (Tokyo, Japan) with a Cu Kα X-ray source (λ = 1.540598 Å). Diffraction patterns were recorded using a D/teX Ultra silicon strip detector (Rigaku) at a speed of 0.05° s^{-1} up to 2θ = 80°, where θ is the angle of incidence. SEM and electron-probe microanalysis were performed using a JXA-8530F instrument (JEOL Ltd., Japan) at an operating voltage of 10 kV. Raman spectroscopy was conducted using a multichannel Raman imaging system (ST Japan Inc., Japan) at an incident wavelength of 532 nm. Transmission electron microscopy (TEM) and scanning TEM (STEM) images were captured using a JEM-2100F TEM/STEM (JEOL Ltd., Japan) equipped with an EDX spectrometer operating at 200 kV. Double-spherical aberration (C_s) correctors (CEOS GmbH, Heidelberg, Germany) were used to obtain high-contrast images with a point-to-point resolution of 1.4 Å. EDX profiles were collected using a JEOL JED-2300 T instrument. X-ray photoelectron spectroscopy (XPS) measurements were conducted using a JPS 9010 TR spectrometer (JEOL Ltd., Japan) equipped with a Mg Kα X-ray source (λ = 1253.6 eV). To that end, the pass energy was set to 10 eV, and each sample was placed on a piece of graphite tape. Because charge accumulation in the sample shifted the binding energy to higher values, the charge-up magnitude was calibrated using the C 1s peaks of graphene and graphite tape at 284.6 eV.

ACCEPTED MANUSCRIPT

2.6 Calculation of crystal size

The crystal size of the powder materials was calculated using the Scherrer equation (2.1).

$$Crystal\ Size\ = \frac{K\lambda}{\beta \cos\theta}, \qquad (2.1)$$

where K is a dimensionless shape factor, typically considered as ~0.9; λ is the X-ray wavelength (1.54060 Å (Cu Kα_1) in this study); θ is the incidence angle of X-ray with respect to the sample holder; β is the full width at half maximum intensity of the peak.

2.7 Electrochemical measurements

All electrochemical measurements were performed using a Corrtest CS2350H electrochemical workstation in aqueous 0.5 M H_2SO_4. The standard three-electrode setup comprised an active-material-loaded glassy carbon electrode (GCE) as the working electrode, a carbon rod as the counter electrode, and Ag/AgCl as the reference electrode. Except for the active material, all the electrodes were purchased from BAS Inc., Japan. For each measurement, the prepared ink (15 μL) was dropped thrice onto the polished surface of the GCE to achieve a final catalyst loading of 0.05 mg cm^{-2}. Linear sweep voltammetry (LSV) curves were recorded at a scan rate of 5 mV s^{-1}.

All experiments were conducted at ambient temperature (298 ± 2 K), and the potentials were evaluated against the reversible hydrogen electrode (RHE) using equation (2.2).

$$E_{RHE} = E_{Ag/AgCl} + 0.059 \times pH + E^0_{Ag/AgCl}$$

$$= E_{Ag/AgCl} + 0.059 \times 0 + E^0_{Ag/AgCl}$$

$$= E_{Ag/AgCl} + 0.199\ V \text{ (at pH 0)}, \qquad (2.2)$$

ACCEPTED MANUSCRIPT

where $E_{Ag/AgCl}$ is the measured potential, and $E^0_{Ag/AgCl}$ is the standard potential of Ag/AgCl (saturated KCl) at 25 °C (0.199 V).

The thermodynamic potential for the HER is 0 V; therefore, the absolute value of the potential obtained by LSV is the overpotential. To better elucidate the HER kinetics, Tafel slopes were derived from the LSV plots. To evaluate the electrocatalytic stability of the catalysts, the LSV curves before and after 6000 CV cycles (0.1 to −0.3 V vs. RHE) at a scan rate of 100 mV s^{-1} were compared.

3. Results and discussion

3.1 Characterization of ball-milled MoS_2

Ball milling is a straightforward, effective method for exfoliating and decreasing the lateral dimensions of large quantities of layered materials. As shown in Figure 1, an industrial milling machine was used to produce small flakes of MoS_2 with different thicknesses, starting from large grains of natural MoS_2, followed by the addition of graphene to increase conductivity and realize superior electrocatalytic performance. SEM was performed to examine the milling-induced morphological changes. As shown in Figure 2, smaller MoS_2 particles were produced via ball milling. Furthermore, XRD was conducted to evaluate the crystal structure and crystal size of each sample (Figure 3), with the Scherrer equation used for the calculations. The results (Table 1) indicated that there was no appearance of the other crystal structure, and the crystal size of MoS_2 gradually reduced from 68 to 4 nm by ball milling.

ACCEPTED MANUSCRIPT

High-resolution STEM was performed to further evaluate the structural properties of ball-milled MoS_2. As shown in Figure 4a and b, the MoS_2-30 min and MoS_2-2 h samples were well crystallized and contained folded, bent layers. Notably, the 2H phase is the most common and stable configuration of MoS_2 [26]. When MoS_2 is multi-layered, the most stable phase is the 2H phase, and when it is single-layered, it is the 1H phase [29]. The difference in the structures of the 1T and 1H phases was identified by the contrast difference as reported previously [29]. The part captured in the photographs is single-layer MoS_2; therefore, it is the 1H phase. According to the atomic structure model, the 1H and 1T phases existed simultaneously in the MoS_2-12 h sample (Figure 4c and d), suggesting that ball milling caused the formation of the 1T phase, presumably through exfoliation.

Further insights into the surface compositions of the materials were obtained by XPS. Specifically, the wide-scan compositional spectra of MoS_2 (Figure S1) and the high-resolution Mo 3d and S 2p spectra (Figure S2) were acquired before and after milling for comparison. Notably, Si was detected in addition to Mo and S in the wide-scan spectra (Figure S1); Si originated from SiO_2, which inevitably emerged during the XPS measurements as the samples were prepared by dripping the sample ink onto a glass slide. The high-resolution Mo 3d and S 2p XPS profiles (Figure S2) showed typical Mo 3d spectra for bulk MoS_2, with sharp signals at approximately 229.5 and 232.6 eV, corresponding to Mo^{4+} $3d_{5/2}$ and Mo^{4+} $3d_{3/2}$, respectively. After ball milling, the MoS_2-12 h sample exhibited a wider spectrum with peaks that shifted to higher energies. This can be ascribed to the presence of Mo atoms with higher oxidation states—that is, Mo^{5+} and Mo^{6+} [30,31]—which result from an oxidative process occurring during ball milling. Notably, a shift in the Mo 3d peaks toward higher energies has been

ACCEPTED MANUSCRIPT

recorded in the presence of high surface-step densities [32]. Ball milling likely produced several surface step edges and defects while reducing the lateral size of the thin film. Similar conclusions were drawn from the S 2p spectra acquired before and after ball milling: the appearance of oxidized higher peak components in S 2p results in broader peaks possibly owing to the oxidation of surface sulfur because of ball milling.

Elemental quantification was performed by acquiring narrow-scan XPS profiles, and the atomic percentage of each element was estimated (Table 2). The S/Mo ratio decreased slightly with increasing ball-milling time, and the longer the ball-milling time, the higher the sulfur defect; this implies that the milling did not induce a significant chemical transformation but created certain sulfur defects that potentially favored electrochemical reactions [33,34,35].

3.2 Electrochemical performance

The electrocatalytic performances of the prepared HER catalysts were tested in a 0.5 M N_2-saturated H_2SO_4 solution at a rotating speed of 1600 rpm. The electrochemical performance analysis of MoS_2 samples ball-milled for different durations, with respect to commercial Pt/C as the reference (Figure S3), showed that the polarization curve gradually shifted to the right after ball milling. This implied that the overpotential decreased, signifying that ball milling undeniably improved the catalytic activity of MoS_2. However, samples ball-milled for longer durations did not always exhibit superior activity. In particular, the 8 h and 12 h ball-milled samples performed worse than the other ball-milled samples. Based on the information obtained from SEM, the smaller MoS_2 particles produced after prolonged ball-milling

ACCEPTED MANUSCRIPT

agglomerated, which likely caused the exposed edges to be covered, thereby reducing the number of active sites and resulting in poor performance.

To disperse the agglomerated particles and thereby obtain catalysts with superior performance, four of the samples were subjected to an additional two hours of bath sonication. As shown in Figure S4 and Table S1, the properties of each sample improved after sonication. Moreover, the longer the ball-milling duration—or alternatively, the smaller the particles—the greater the improvement after the additional sonication. Sonication caused the agglomerated particles to redisperse, exposing more edges and thereby improving the catalytic activity. Furthermore, the samples ball-milled for longer durations exposed more edges than those of the samples subjected to shorter ball-milling periods; additionally, the ball-milling process produced the 1T phase (Figure 4) and sulfur defects (Table 2). These results are consistent with previous discussions on the active sites of MoS_2; thus, the presence of more exposed edges, the 1T phase, and sulfur vacancies is imperative to the HER catalyzing activity [14,15,18].

CV measurements were conducted in the presence of ferro/ferricyanide cyanide as an oxidation–reduction probe to evaluate the heterogeneous electron transfer between the material and the ferro/ferri ions in the solution. As shown in Figure S5, the CV profile of MoS_2-12 h differed only slightly from that of bulk MoS_2. Notably, the oxidation and reduction current intensities of the redox probe increased by ~25%, presumably owing to the ball-milling-induced increase and decrease in the electrochemical surface area and particle size of the material, respectively. Additionally, slightly faster electron transfer occurred after ball milling, resulting in less peak-to-peak separation between the oxidation and reduction profiles

ACCEPTED MANUSCRIPT

of the reducing probe. This was also potentially due to the increased availability of the edge components, which have been proven to be remarkably potent active sites [36].

The as-prepared MoS_2 samples were subsequently integrated with graphene—a typical conductive material—to improve their activity further [37,38]; this also helped maintain the morphology of the exfoliated sheets. As shown in Figure S6 and Table S2, the mixture of ball-milled MoS_2 and graphene (MoS_2 + G) samples exhibited superior performance. In particular, the MoS_2-12 h + G sample showed an overpotential (160 mV) that was ~335 mV lower than that of pristine bulk MoS_2. This enhanced activity can be ascribed to the improved electronic conductivity and suppressed agglomeration of MoS_2 particles by mixing with flexible graphene: as shown in Figure S7, an SEM-based morphological analysis of MoS_2-12 h + G shows that graphene plays an important role in connecting MoS_2 and the electrode as well as the spacer to prevent agglomeration. Furthermore, the only-graphene sample exhibited low activity, and comparing the CV cycles with a large range of potential (Figure S8), there is a distinct difference in the current densities between the only-graphene sample and MoS_2-12 h + G sample, thereby confirming the important role of graphene in providing conductivity. A performance comparison was performed between bulk MoS_2 and the sonicated and graphene-incorporated variants of MoS_2-12 h (Figure 5 and Table S3). The MoS_2-12 h + G sample exhibited improved performance, with a lower overpotential and a smaller Tafel slope. The decrease in the Tafel slope of MoS_2-12 h + G may be due to the introduction of graphene-supported conductivity in the materials (in other words, the larger Tafel slope is due to low conductivity), and the smaller Tafel slope also indicates its superior kinetics. Based on this finding, the graphene addition had a better effect on the catalyst performance than

ACCEPTED MANUSCRIPT

sonication, presumably because graphene not only increased the electronic conductivity of the sample but also helped maintain the morphology and exposed edge state of MoS_2 [39,40,41]. Furthermore, MoS_2-12 h + G outperforms several other noteworthy MoS_2-based electrocatalysts in the HER (Table S4 and Figure S9) [42,43,44,45,46,47,48]. Although certain catalysts exhibit better performance, they require additional and more complex procedures for operation. Therefore, the method used to prepare the graphene-integrated ball-milled MoS_2 is more cost-effective than several other techniques[34,49,50,51].

Stability is another key factor in the evaluation of electrocatalysts. The electrochemical stability of MoS_2-12 h + G was evaluated by comparing the LSV curves before and after 6000 CV cycles. As shown in Figure 5c, the MoS_2-12 h + G sample cycled 6000 times continued to exhibit high catalytic activity, and the overpotential at 10 mA cm^{-2} shifted by only 15 mV, suggesting its superior stability. Furthermore, the morphology of the MoS_2-12 h + G sample did not change after the stability measurements (Figure S10). The surface elemental composition after 6000 CV cycles was evaluated by XPS (Figure S11), and the results revealed only a slight shift in the peaks after the long-term stability measurements, which were evidently due to slight oxidation on the surface. Collectively, these findings underscore the remarkable potential of the electrochemically stable graphene-incorporated ball-milled MoS_2 for future applications.

4. Conclusion

In this study, the size of MoS_2 particles was controlled using a simple mechanical process—ball milling—and the as-prepared samples exhibited significantly enhanced electrochemical and catalytic properties compared to those of pristine bulk MoS_2. Upon ball milling, a 25%

ACCEPTED MANUSCRIPT

enhancement was observed in the current intensity, and peak-to-peak separation was achieved. The HER activity of the as-prepared ball-milled sample was further improved by introducing graphene. In particular, the MoS_2-12 h + G sample exhibited superior performance, showing an overpotential (160 mV) that was ~335 mV lower than that of pristine bulk MoS_2. These improved performance metrics were most likely due to the increased availability and density of edge planes in the material, which was achieved by the particle size reduction, the appearance of the 1T phase, and an increase in sulfur vacancies, in addition to the superior bolstering effect of graphene. Therefore, ball milling with graphene mixture shows promise as a new, scalable method for preparing size-controlled, highly active electrocatalysts.

Acknowledgments

The authors are grateful to Prof. Takeaki Sakurai and Dr. S. A. Pawar from the University of Tsukuba for providing experimental support during the early stages of this study. This study was supported by the Japan Science and Technology Agency (JST) through the Adaptable and Seamless Technology Transfer Program through Target-driven R&D (A-STEP) [grant number JPMJTR22T4]; JSPS KAKENHI [grant numbers JP19H02551, JP19H05790, JP19H05046:A01, JP21H00015:B01, JP21H05012, JP22K18964, JP23K26536, and JP23H01843]; and MHI Innovation Accelerator LLC.

ACCEPTED MANUSCRIPT

References

[1] Chow J, Kopp RJ, Portney PR. Energy resources and global development. Science. 2003;302(5650):1528–1531.

[2] Crabtree GW, Dresselhaus MS, Buchanan MV. The hydrogen economy. Phys Today. 2004;57(12):39–44.

[3] Turner JA. A realizable renewable energy future. Science. 1999;285(5428):687–689.

[4] Dawood F, Anda M, Shafiullah GM. Hydrogen production for energy: an overview. Int J Hydrogen Energy. 2020;45(7):3847–3869.

[5] Tafel J. Über die Polarisation bei kathodischer Wasserstoffentwicklung [On the polarization during cathodic hydrogen evolution]. Z Phys Chem. 1905;50U:641–712.

[6] Wang S, Lu A, Zhong CJ. Hydrogen production from water electrolysis: role of catalysts. Nano Convergence. 2021;8:4.

[7] Dubouis N, Grimaud A. The hydrogen evolution reaction: from material to interfacial descriptors. Chem Sci. 2019;10(40):9165–9181.

[8] Lasia A. Mechanism and kinetics of the hydrogen evolution reaction. Int J Hydrogen Energy. 2019;44(36):19484–19518.

[9] Shi Y, Zhang B. Recent advances in transition metal phosphide nanomaterials: synthesis and applications in hydrogen evolution reaction. Chem Soc Rev. 2016;45(6):1529–1541.

[10] Wang D, Wang Z, Wang C, et al. Distorted MoS_2 nanostructures: an efficient catalyst for the electrochemical hydrogen evolution reaction. Electrochem Commun. 2013;34:219–222.

[11] Yan K, Lu Y. Direct growth of MoS_2 microspheres on Ni foam as a hybrid nanocomposite efficient for oxygen evolution reaction. Small. 2016;12(22):2975–2981.

[12] Voiry D, Salehi M, Silva R, et al. Conducting MoS_2 nanosheets as catalysts for hydrogen evolution reaction. Nano Lett. 2013;13(12):6222–6227.

[13] Jaramillo TF, Jørgensen KP, Bonde J, et al. Identification of active edge sites for electrochemical H_2 evolution from MoS_2 nanocatalysts. Science. 2007;317(5834):100–102.

[14] Zhang J, Wu J, Guo H, et al. Unveiling active sites for the hydrogen evolution reaction on monolayer MoS_2. Adv Mater. 2017;29(42):1701955.

[15] Yin Y, Han J, Zhang Y, et al. Contributions of phase, sulfur vacancies, and edges to the hydrogen evolution reaction catalytic activity of porous molybdenum disulfide nanosheets. J Am Chem Soc. 2016;138(25):7965–7972.

ACCEPTED MANUSCRIPT

[16] Lukowski MA, Daniel AS, Meng F, et al. Enhanced hydrogen evolution catalysis from chemically exfoliated metallic MoS_2 nanosheets. J Am Chem Soc. 2013;135(28):10274–10277.

[17] Tan Y, Liu P, Chen L, et al. Monolayer MoS_2 films supported by 3D nanoporous metals for high-efficiency electrocatalytic hydrogen production. Adv Mater. 2014;26(47):8023–8028.

[18] Li G, Zhang D, Qiao Q, et al. All the catalytic active sites of MoS_2 for hydrogen evolution. J Am Chem Soc. 2016;138(51):16632–16638.

[19] Ambrosi A, Chia X, Sofer Z, et al. Enhancement of electrochemical and catalytic properties of MoS_2 through ball-milling. Electrochem Commun. 2015;54:36–40.

[20] Maijenburg AW, Regis M, Hattori AN, et al. MoS_2 nanocube structures as catalysts for electrochemical H_2 evolution from acidic aqueous solutions. ACS Appl Mater Interfaces. 2014;6(3):2003–2010.

[21] Chen Z, Forman AJ, Jaramillo TF. Bridging the gap between bulk and nanostructured photoelectrodes: the impact of surface states on the electrocatalytic and photoelectrochemical properties of MoS_2. J Phys Chem C. 2013;117(19):9713–9722.

[22] Chung DY, Park SK, Chung YH, et al. Edge-exposed MoS_2 nano-assembled structures as efficient electrocatalysts for hydrogen evolution reaction. Nanoscale. 2014;6(4):2131–2136.

[23] Joensen P, Frindt RF, Morrison SR. Single-layer MoS_2. Mater Res Bull. 1986;21(4):457–461.

[24] Coleman JN, Lotya M, O'Neill A, et al. Two-dimensional nanosheets produced by liquid exfoliation of layered materials. Science. 2011;331(6017):568–571.

[25] Voiry D, Yamaguchi H, Li J, et al. Enhanced catalytic activity in strained chemically exfoliated WS_2 nanosheets for hydrogen evolution. Nat Mater. 2013;12(9):850–855.

[26] Wang D, Zhang X, Bao S, et al. Phase engineering of a multiphasic 1T/2H MoS_2 catalyst for highly efficient hydrogen evolution. J Mater Chem A. 2017;5(6):2681–2688.

[27] Eda G, Yamaguchi H, Voiry D, et al. Photoluminescence from chemically exfoliated MoS_2. Nano Lett. 2011;11(12):5111–5116.

ACCEPTED MANUSCRIPT

[28] Wang T, Liu L, Zhu Z, et al. Enhanced electrocatalytic activity for hydrogen evolution reaction from self-assembled monodispersed molybdenum sulfide nanoparticles on an Au electrode. Energy Environ Sci. 2013;6(2):625–633.

[29] Eda G, Fujita T, Yamaguchi H, et al. Coherent atomic and electronic heterostructures of single-layer MoS_2, ACS Nano. 2012;6(8):7311–7317.

[30] Choi JG, Thompson LT. XPS study of as-prepared and reduced molybdenum oxides. Appl Surf Sci. 1996;93(2):143–149.

[31] Al-Kandari H, Al-Kharafi F, Al-Awadi N, et al. The catalytic active sites in partially reduced MoO_3 for the hydroisomerization of 1-pentene and *n*-pentane. Appl Catal A. 2005;295(1):1–10.

[32] Mahatha SK, Menon KSR. Inhomogeneous band bending on MoS_2 (0001) arising from surface steps and dislocations. J Phys: Condens Matter. 2012;24(30):305502.

[33] Cheng Y, Song H, Wu H, et al. Defects enhance the electrocatalytic hydrogen evolution properties of MoS_2-based materials. Chem Asian J. 2020;15(20):3123–3134.

[34] Joyner J, Oliveria EF, Yamaguchi H, et al. Graphene supported MoS_2 structures with high defect density for an efficient HER electrocatalysts. ACS Appl Mater Interfaces. 2020;12(11):12629–12638.

[35] Wang X, Zhang Y, Si H, et al. Single-atom vacancy defect to trigger high-efficiency hydrogen evolution of MoS_2. J Am Chem Soc. 2020;142(9):4298–4308.

[36] Ahmed SM, Gerischer H. Influence of crystal surface orientation on redox reactions at semiconducting MoS_2. Electrochim Acta. 1979;24(6):705–711.

[37] Li L, Hagiwara S, Jiang C, et al. Boron monosulfide as an electrocatalyst for the oxygen evolution reaction, Chem Eng J. 2023;471:144489.

[38] Li L, Watanabe N, Jiang C, et al. Development of a highly stable nickel-foam-based boron monosulfide–graphene electrocatalyst with a high current density for the oxygen evolution reaction, Sci Technol Adv Mater. 2023;24(1):2277681.

[39] Meng X, Yu L, Ma C, et al. Three-dimensionally hierarchical MoS_2/graphene architecture for high-performance hydrogen evolution reaction. Nano Energy. 2019;61:611–616.

ACCEPTED MANUSCRIPT

[40] Liao L, Zhu J, Bian X, et al. MoS_2 formed on mesoporous graphene as a highly active catalyst for hydrogen evolution. Adv Funct Mater. 2013;23(42):5326–5333.

[41] Behera SK, Deb P, Ghosh A. Mechanistic study on electrocatalytic hydrogen evolution by high efficiency graphene/MoS_2 heterostructure. ChemistrySelect. 2017;2(13):3657–3667.

[42] Liu Z, Gao Z, Liu Y, et al. Heterogeneous nanostructure based on 1T-phase MoS_2 for enhanced electrocatalytic hydrogen evolution. ACS Appl Mater Interfaces. 2017;9(30):25291–25297.

[43] Liu Z, Zhao L, Liu Y, et al. Vertical nanosheet array of 1T phase MoS_2 for efficient and stable hydrogen evolution. Appl Catal B. 2019;246:296–302.

[44] Yao Y, Ao K, Lv P, et al. MoS_2 coexisting in 1T and 2H phases synthesized by common hydrothermal method for hydrogen evolution reaction. Nanomaterials. 2019;9(6):844.

[45] Li Y, Yin K, Wang L, et al. Engineering MoS_2 nanomesh with holes and lattice defects for highly active hydrogen evolution reaction. Appl Catal B. 2018;239:537–544.

[46] Eftekhari A. Electrocatalysts for hydrogen evolution reaction. Int J Hydrogen Energy. 2017;42(16):11053–11077.

[47] Murthy AP, Madhavan J, Murugan K. Recent advances in hydrogen evolution reaction catalysts on carbon/carbon-based supports in acid media. J Power Sources. 2018;398:9–26.

[48] Chen B, Hu P, Yang F, et al. In situ porousized MoS_2 nano islands enhance HER/OER bifunctional electrocatalysis. Small. 2023;19(14):2207177.

[49] Mugheri AQ, Otho AA, Mugheri AA. Meritorious spatially on hierarchically Co_3O_4/MoS_2 phase nanocomposite synergistically a high-efficient electrocatalyst for hydrogen evolution reaction performance: recent advances & future perspectives. Int J Hydrogen Energy. 2021;46(44):22707–22718.

[50] Bolar S, Shit S, Murmu NC, et al. Activation strategy of MoS_2 as HER electrocatalyst through doping-induced lattice strain, band gap engineering, and active crystal plane design. ACS Appl Mater Interfaces. 2021;13(1):765–780.

ACCEPTED MANUSCRIPT

[51] Guo D, Wan Z, Fang G, et al. A tandem interfaced (Ni_3S_2-MoS_2)@TiO_2 composite fabricated by atomic layer deposition as efficient HER electrocatalyst. Small. 2022;18(24):2201896.

ACCEPTED MANUSCRIPT

Figures, tables, and captions

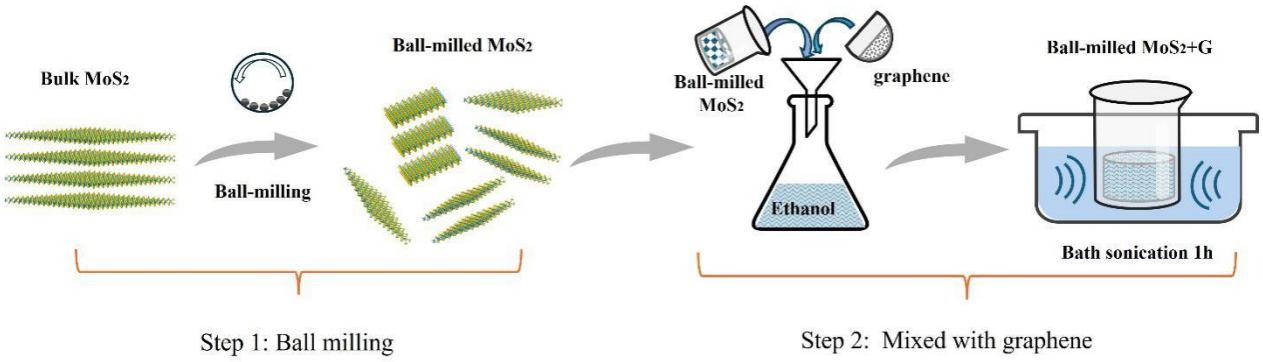

Figure 1. Synthesis of graphene-integrated ball-milled MoS_2 electrocatalyst.

ACCEPTED MANUSCRIPT

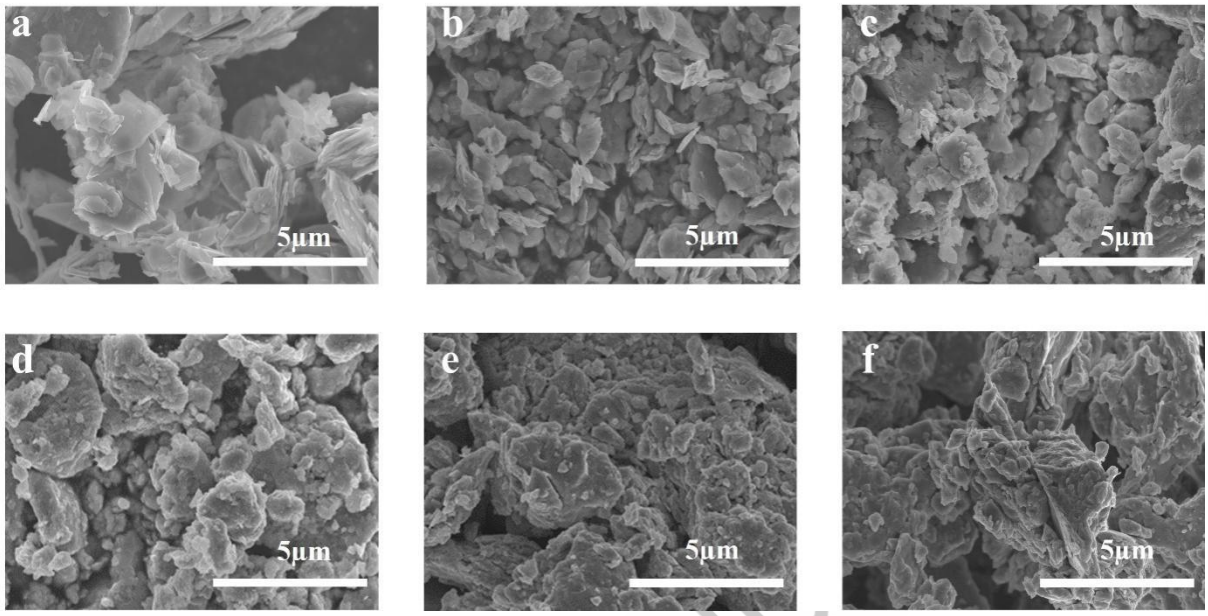

Figure 2. SEM images of (a) pristine bulk MoS_2, (b) MoS_2-30 min, (c) MoS_2-2 h, (d) MoS_2-4 h, (e) MoS_2-8 h, and (f) MoS_2-12 h.

ACCEPTED MANU

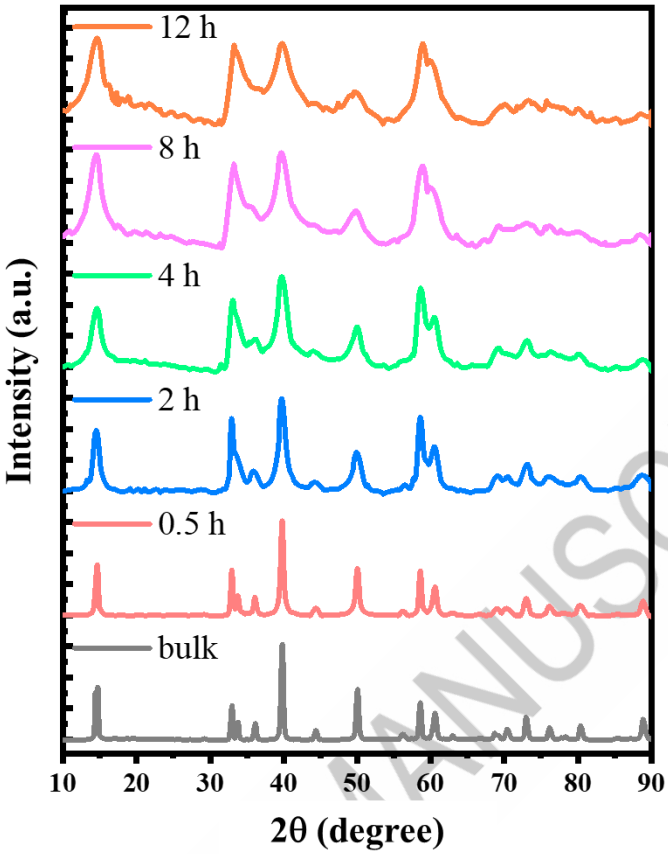

Figure 3. XRD patterns of bulk MoS_2 powder and MoS_2 samples ball-milled for different durations.

ACCEPTED MANUSCRIPT

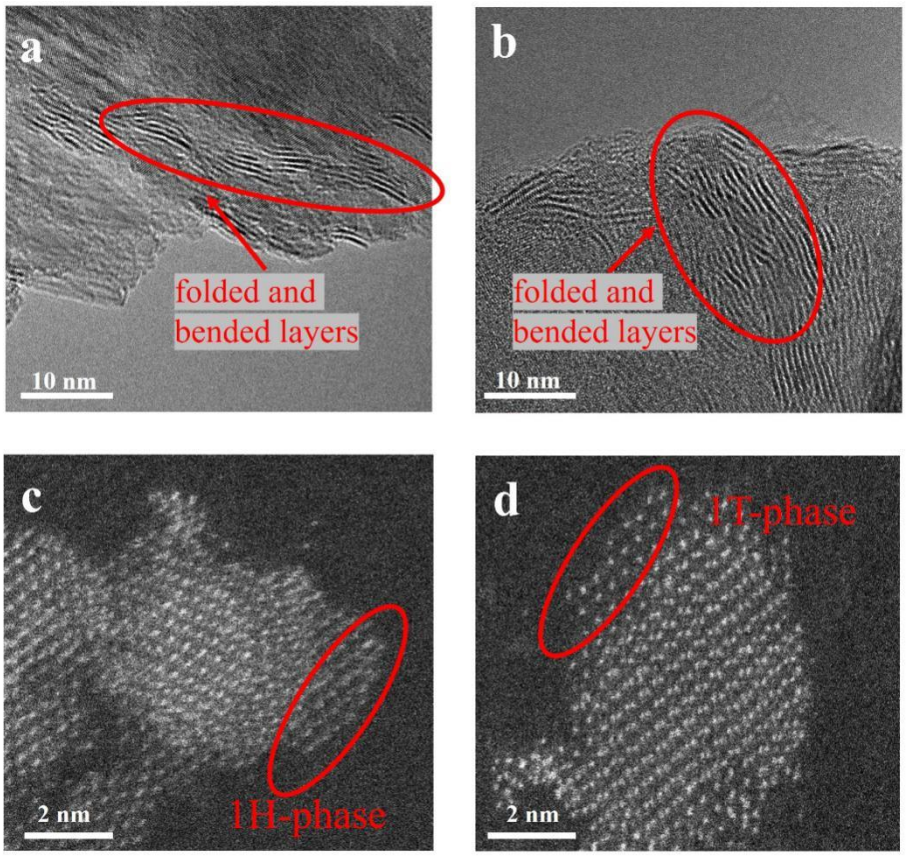

Figure 4. STEM images of (a) MoS_2-30 min and (b–d) MoS_2-12 h.

ACCEPTED MANUSCRIPT

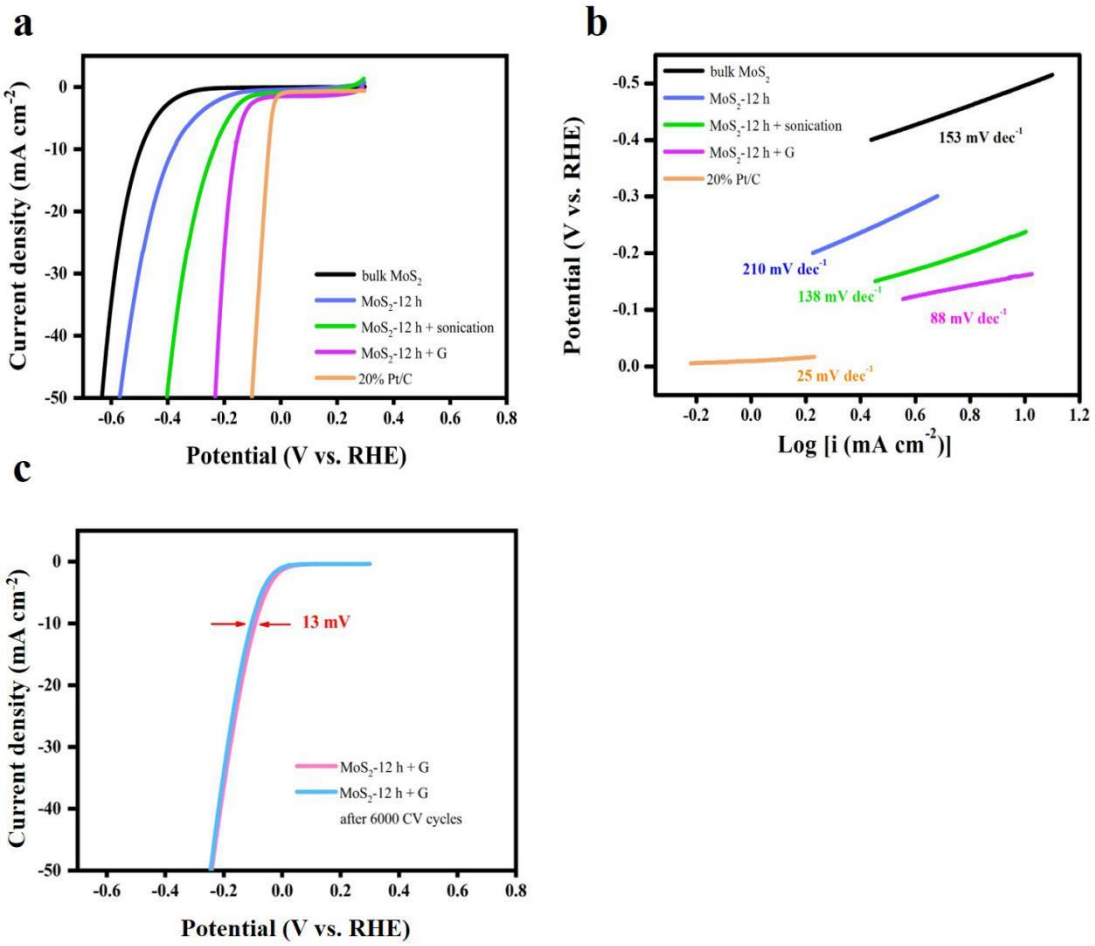

Figure 5. (a) LSV curves for HER with the as-prepared MoS_2 samples in aqueous 0.5 M H_2SO_4, and (b) corresponding Tafel plots. (c) LSV curves of the MoS_2-12 h + G electrocatalyst recorded before and after 6000 cyclic voltammetry cycles (0.1 to −0.3 V vs. RHE) in aqueous 0.5 M H_2SO_4.

ACCEPTED

Table 1. Crystal sizes of MoS_2 samples ball-milled for varying periods, calculated using the Scherrer equation.

Sample	2θ (degree)	FWHM	Crystallite size (nm)
Bulk MoS_2	13.63	0.12	68
MoS_2-15 min	14.05	0.23	35
MoS_2-30 min	14.03	0.30	26
MoS_2-1 h	14.06	0.51	15
MoS_2-2 h	14.05	0.90	8
MoS_2-4 h	14.06	0.98	6
MoS_2-12 h	14.05	1.20	4

ACCEPTED MANUSCRIPT

Table 2. Atomic percentages of the main elements detected by XPS for pristine bulk MoS_2 and MoS_2 samples ball-milled for different durations. The values of Mo and S are derived from the areas of the Mo 3d peak and S 2p peaks with sensitivities (Mo 3d5/2:23.52 and S 2p3/2:7.18) determined using SpecSurf software (JEOL Ltd., Japan).

Sample (MoS_2)	**Mo (at%)**	**S (at%)**	**S/Mo ratio**	**MoS_2 (S/Mo: 2/1)**
Bulk	44.6	55.4	1.24	2.00
Ball-milled 30 min	45.6	54.4	1.19	1.92
Ball-milled 1 h	46.5	53.5	1.15	1.85
Ball-milled 2 h	46.9	53.1	1.13	1.82
Ball-milled 4 h	47.5	52.5	1.10	1.77
Ball-milled 12 h	48.2	51.8	1.07	1.72

ACCEPTED MANUSCRIPT

Li et al. reported MoS_2-based electrocatalysts for the hydrogen evolution reaction. The superior catalytic activity was ascribed to exposed edge sites, sulfur vacancies, 1T phase, and the effect of graphene.

ACCEPTED MANUSCRIPT

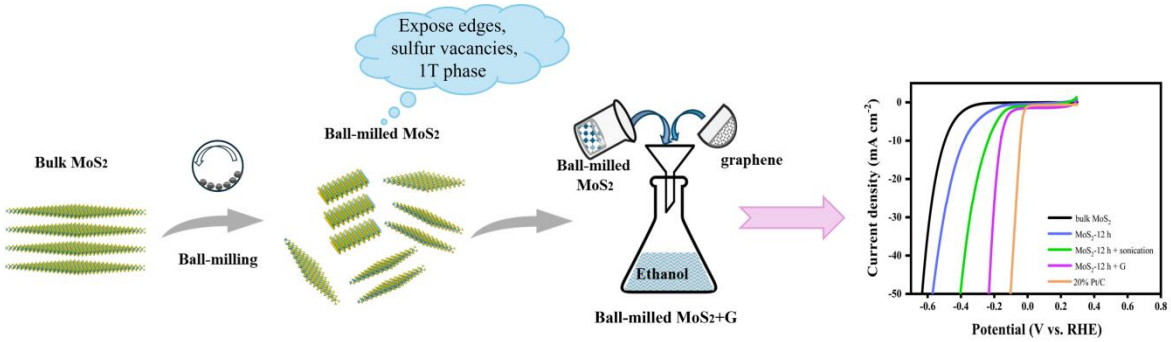

TOC

ACCEPTED MANUSCRIPT

Supplementary information

Ball-milled MoS_2 with graphene shows enhanced catalytic activity for hydrogen evolution reaction

Table of contents

ACCEPTED MANUSCRIPT

Supplementary figures

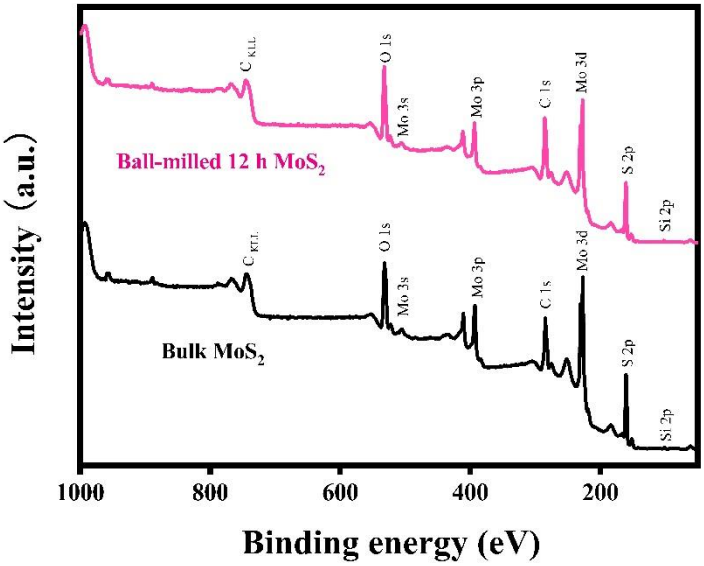

Figure S1. Wide-scan XPS profiles of bulk MoS_2 before (black) and after (pink) ball milling for 12 h. (Si originates from SiO_2, which is inevitably present during the XPS measurements, as each sample is prepared by dripping the sample ink onto a glass slide.)

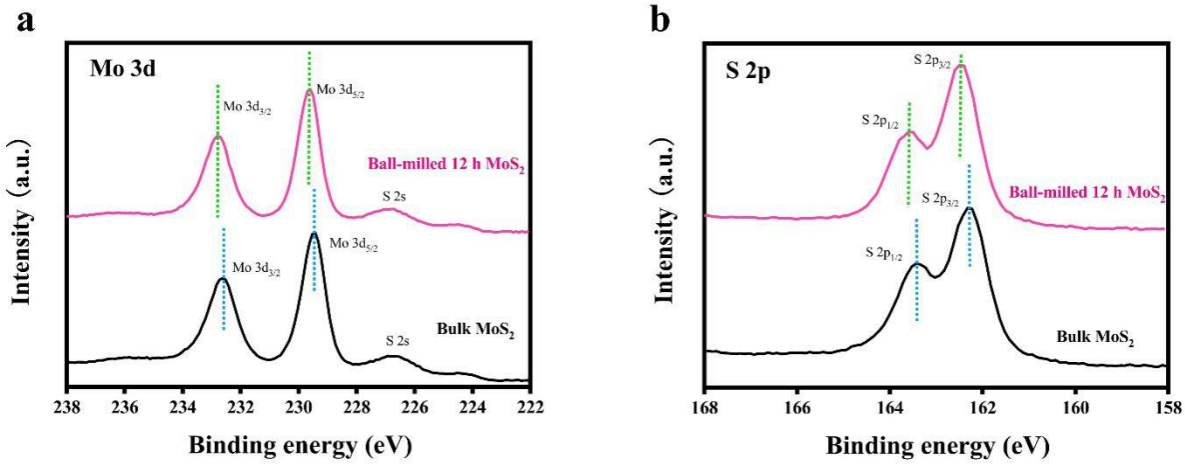

Figure S2. High-resolution (a) Mo 3d and (b) S 2p XPS profiles of bulk MoS_2 before (black) and after (pink) 12 h of ball milling.

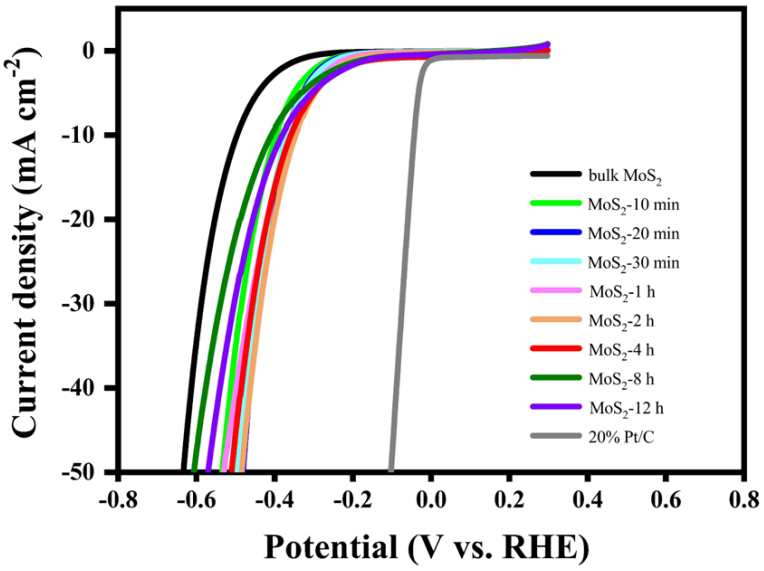

Figure S3. LSV curves of as-prepared ball-milled samples, a commercial 20% Pt/C specimen, and bulk MoS_2 in aqueous 0.5 M H_2SO_4.

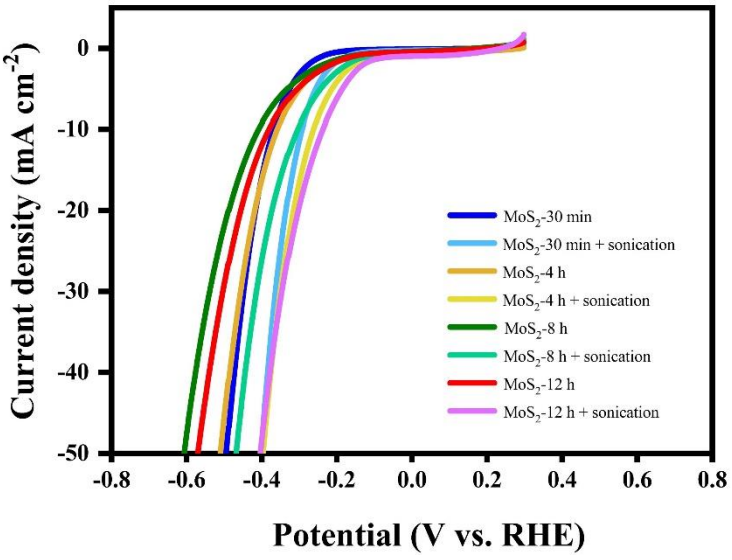

Figure S4. LSV curves for the HER of as-prepared and sonicated samples in aqueous 0.5 M H_2SO_4.

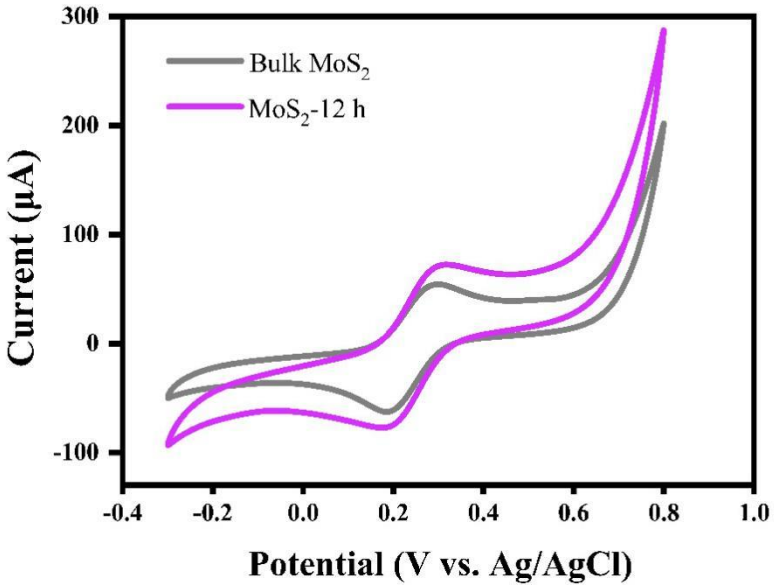

Figure S5. Cyclic voltammograms of 5 mM $[Fe(CN)_6]^{4-/3-}$ (vs. Ag/AgCl reference electrode) using bulk MoS_2 and MoS_2 ball-milled for 12 h, with 0.1 M KCl as the supporting electrolyte.

ACCEPTED MANUSCRIPT

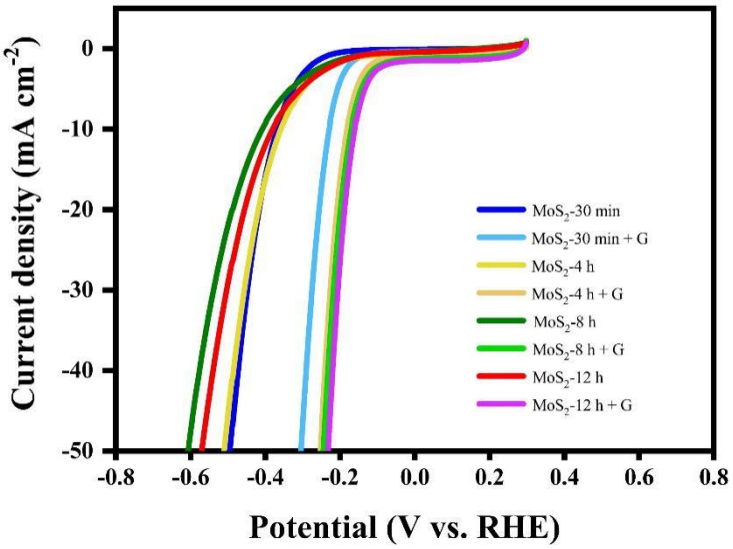

Figure S6. LSV curves for the HER of as-prepared and graphene-incorporated samples in aqueous 0.5 M H_2SO_4.

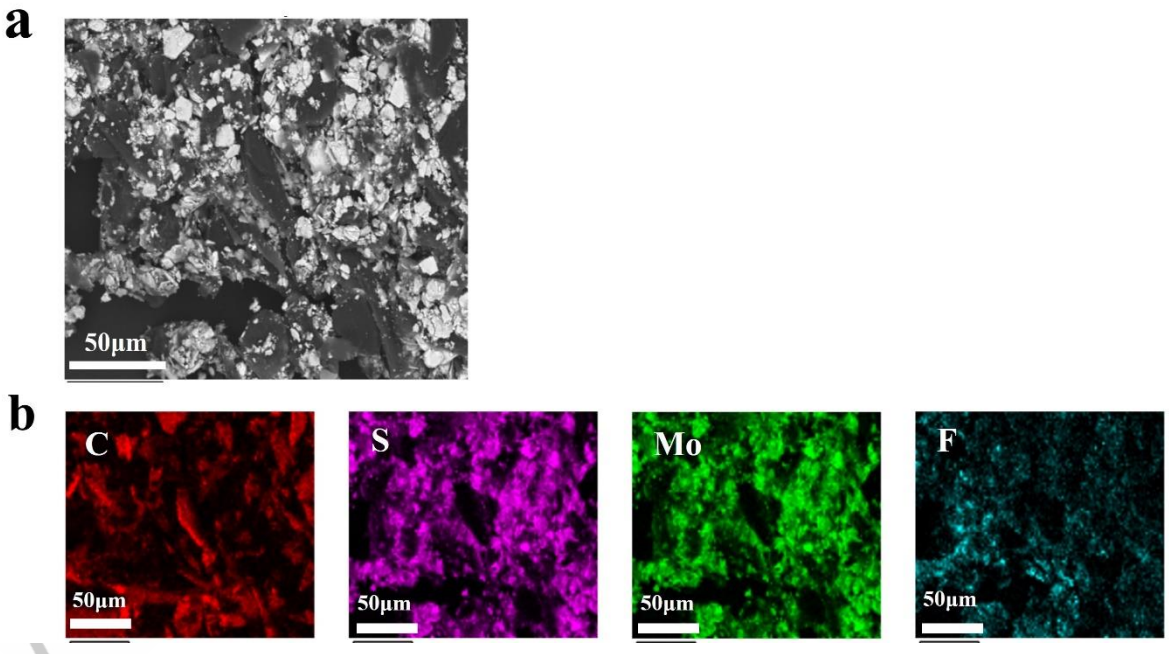

Figure S7. (a) SEM image and (b) electron-probe microanalysis mapping images of MoS_2-12 h + G with Nafion.

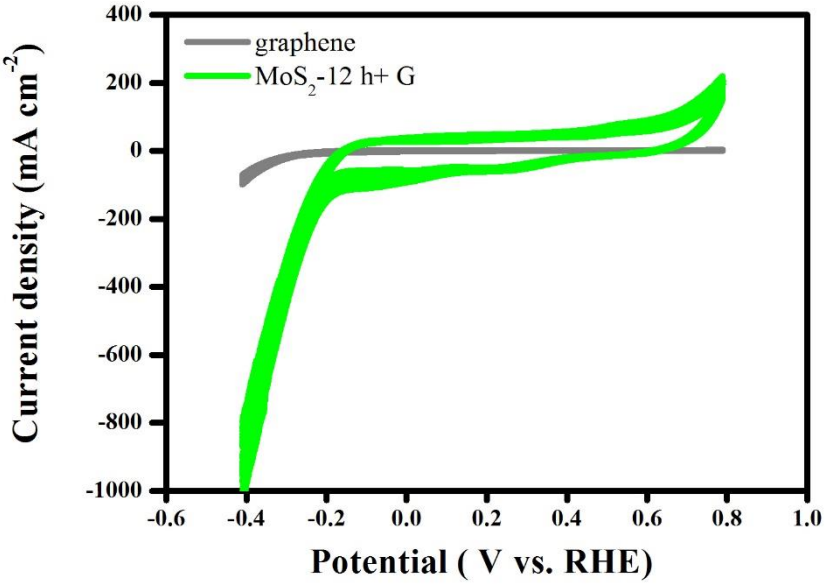

Figure S8. Cyclic voltammograms of graphene and MoS_2 -12 h + G sample in aqueous 0.5 M H_2SO_4.

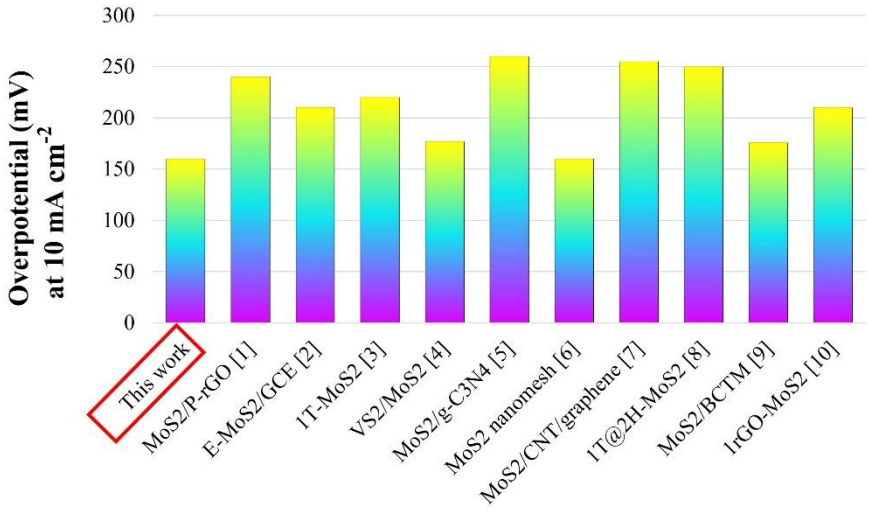

Figure S9. Overpotentials of several MoS_2-based catalysts at a current density of 10 mA cm^{-2} under acidic conditions [1–10].

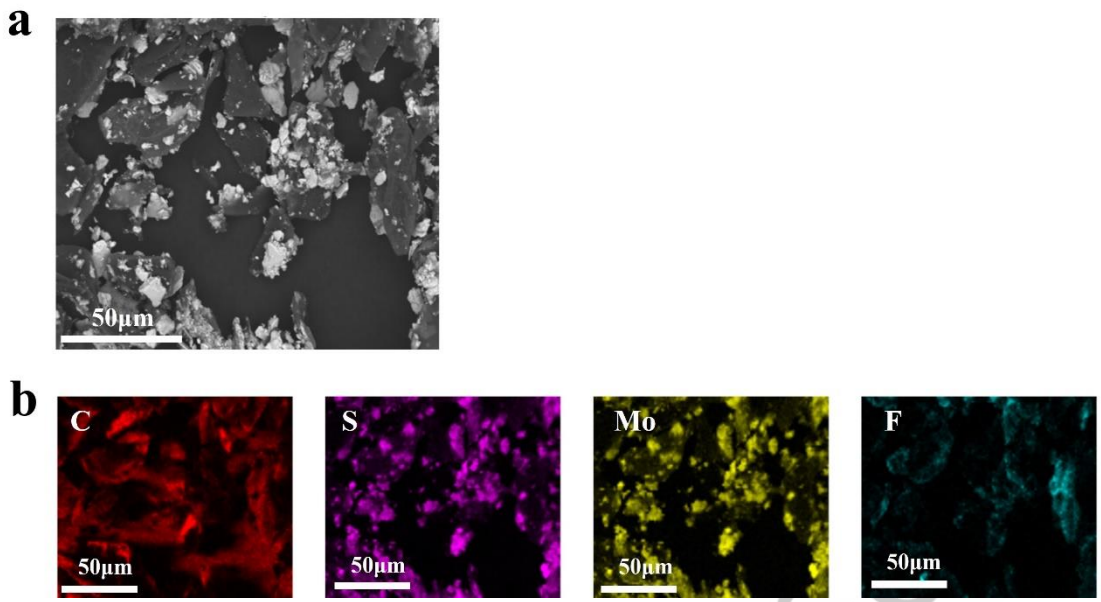

Figure S10. (a) SEM image and (b) electron-probe microanalysis mapping images of MoS_2-12 h + G with Nafion after stability measurements.

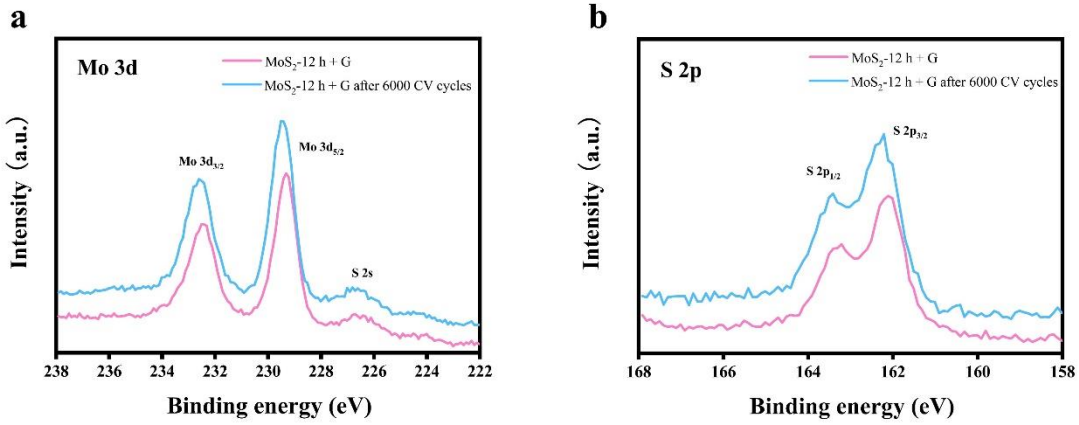

Figure S11. High-resolution (a) Mo 3d and (b) S 2p XPS profiles of MoS_2 ball-milled for 12 h before (pink) and after (blue) 6000 CV cycles.

ACCEPTED MANUSCRIPT

Supplementary tables

Table S1. Comparison of as-prepared and sonicated samples

Sample	Overpotential at 10 mA cm^{-2} (mV)		Sample (with 2 h sonication)	Overpotential at 10 mA cm^{-2} (mV)
MoS_2-30 min	368		**MoS_2-30 min + sonication**	292 (76▼)
MoS_2-4 h	359		**MoS_2-4 h + sonication**	262 (97▼)
MoS_2-8 h	408		**MoS_2-8 h + sonication**	304 (104▼)
MoS_2-12 h	380		**MoS_2-12 h + sonication**	237 (143▼)

Table S2. Comparison of as-prepared and graphene-integrated samples.

Sample	Overpotential at 10 mA cm^{-2}		Sample (mixed with graphene)	Overpotential at 10 mA cm^{-2} (mV)

ACCEPTED MANUSCRIPT

	(mV)			
MoS_2-30 min	368		**MoS_2-30 min + G**	228 (140▼)
MoS_2-4 h	359		**MoS_2-4 h + G**	180 (179▼)
MoS_2-8 h	408		**MoS_2-8 h + G**	169 (239▼)
MoS_2-12 h	380		**MoS_2-12 h + G**	160 (220▼)

Table S3. Comparison of certain as-prepared, and sonicated, and graphene-incorporated samples

Sample	**Overpotential at 10 mA cm^{-2} (mV)**	**Tafel slope (mV dec^{-1})**
Bulk MoS_2	495	146
MoS_2-12 h	380	200
MoS_2-12 h + sonication	237	129
MoS_2-12 h + G	160	86
20% Pt/C	44	25

ACCEPTED MANUSCRIPT

Table S4. Comparison of the HER performances of previously reported MoS_2-based electrocatalysts in acidic solutions.

	Overpotential at 10 mA cm^{-2} (mV)	**Tafel slope ($mV\ dec^{-1}$)**	**Reference**
MoS_2-12 h + G	160	86	This work
MoS_2/P-rGO	240	75	[1]
E-MoS_2/GCE	210	70	[2]
GQDs-MoS_2	200	43	[3]
1T-MoS_2	220	61	[4]
VS_2/MoS_2	177	55	[5]
MoS_2/g-C_3N_4	260	63	[6]
MoS_2 nanomesh	160	46	[7]
MoS_2/CNT/graphene	255	100	[8]
1T@2H-MoS_2	250	88	[9]
MoS_2/BCTM	176	51	[10]
1rGO-MoS_2	210	41	[11]
MoS_2 nano islands	248	84	[12]

ACCEPTED MANUSCRIPT

References

[1] Liu Y, Liu J, Li Z, et al. Exfoliated MoS_2 with porous graphene nanosheets for enhanced electrochemical hydrogen evolution. Int J Hydrogen Energy. 2018;43(30):13946–13952.

[2] Ji S, Yang Z, Zhang C, et al. Exfoliated MoS_2 nanosheets as efficient catalysts for electrochemical hydrogen evolution. Electrochim Acta. 2013;109:269–275.

[3] Guo J, Zhu H, Sun Y, et al. Doping MoS_2 with graphene quantum dots: structural and electrical engineering towards enhanced electrochemical hydrogen evolution. Electrochim Acta. 2016;211:603–610.

[4] Liu Z, Gao Z, Liu Y, et al. Heterogeneous nanostructure based on 1T-phase MoS_2 for enhanced electrocatalytic hydrogen evolution. ACS Appl Mater Interfaces. 2017;9(30):25291–25297.

[5] Chen X, Yu K, Shen Y, et al. Synergistic effect of MoS_2 nanosheets and VS_2 for the hydrogen evolution reaction with enhanced humidity-sensing performance. ACS Appl Mater Interfaces. 2017;9(48):42139–42148.

[6] Fageria P, Sudharshan KY, Nazir R, et al. Decoration of MoS_2 on g-C_3N_4 surface for efficient hydrogen evolution reaction. Electrochim Acta. 2017;258:1273–1283.

[7] Li Y, Yin K, Wang L, et al. Engineering MoS_2 nanomesh with holes and lattice defects for highly active hydrogen evolution reaction. Appl Catal B. 2018;239:537–544.

[8] Murthy AP, Madhavan J, Murugan K. Recent advances in hydrogen evolution reaction catalysts on carbon/carbon-based supports in acid media. J Power Sources. 2018;398:9–26.

[9] Yao Y, Ao K, Lv P, et al. MoS_2 coexisting in 1T and 2H phases synthesized by common hydrothermal method for hydrogen evolution reaction. Nanomaterials. 2019;9(6):844.

ACCEPTED MANUSCRIPT

[10] Qiao S, Zhao J, Zhang B, et al. Micrometer–scale biomass carbon tube matrix auxiliary MoS_2 heterojunction for electrocatalytic hydrogen evolution. Int J Hydrogen Energy. 2019;44(60):32019–32029.

[11] Joyner J, Oliveira EF, Yamaguchi H, et al. Graphene supported MoS_2 structures with high defect density for an efficient HER electrocatalysts. ACS Appl Mater Interfaces. 2020;12(11)12629–12638.

[12] Chen B, Hu P, Yang F, et al. In situ porousized MoS_2 nano islands enhance HER/OER bifunctional electrocatalysis. Small. 2023;19(14):2207177.

ACCEPTED MANUSCRIPT